Limits of detection of defects near edges of nanostructures for coherent Fourier scatterometry

Anubhav Paul* and Silvania F. Pereira

Imaging Physics Department, Faculty of Applied Sciences, Delft University of Technology, Lorentzweg 1, 2628 CJ Delft, The Netherlands

ABSTRACT

Coherent Fourier scatterometry (CFS) is a non-invasive optical technique widely used for defect detection on planar surfaces. It utilizes split detectors to measure far-field asymmetries as differential signals, making it highly effective for identifying defects such as particles or burrows. Detecting defects near edges of nanostructures, however, is particularly challenging due to interference between the edge signal and the defect signal, a limitation not only of CFS but also of other standard techniques like bright-field and dark-field microscopy. Accurate detection of such defects is critical in fields like semiconductor manufacturing and nanotechnology, where edge-adjacent defects can compromise device performance. Therefore, understanding the limits of CFS for edge-adjacent defect detection is essential for optimizing its application and interpreting its results. In this work, we first demonstrate experimentally that CFS can detect a 200 nm Pt particle positioned 2 μm from an edge. We then perform 3D FDTD simulations to model particles and burrows positioned at varying distances from an edge. By analyzing the split detector signals for these scenarios, we observe that particle and burrow signals become more prominent as their distance from the edge increases. However, for a system using a numerical aperture of 0.9 and wavelength of 633 nm, for distances from the edge smaller than 350 nm for particles and 650 nm for burrows, the characteristic signals diminish, merging with the edge response. This study highlights the challenges and potential solutions for defect inspection near edges, advancing the applicability of CFS for patterned and complex structures.

Keywords: coherent Fourier scatterometry, limitations of detection, defect detection, edge inspection

1. INTRODUCTION

The detection of defects near wafer edges is a longstanding challenge in the semiconductor industry. As critical dimensions continue to shrink, even minor edge-adjacent defects can significantly affect device performance and yield. The wafer edge, bevel, and notch regions often experience complex topography, material transitions, and contamination risks that complicate inspection.[1–3] These regions are also prone to process-induced damages and mechanical stress, increasing the likelihood of defect formation. As such, detecting and characterizing defects in these regions is vital for ensuring reliability and reducing cost.

Traditional techniques for defect detection include scanning electron microscopy (SEM), atomic force microscopy (AFM), and bright-field or dark-field optical inspection. While SEM and AFM provide nanometer-scale resolution, they are typically invasive, slow, and unsuitable for in-line inspection.[4–7] Dark-field optical microscopy, although fast and non-invasive, is limited by diffraction and struggles with scattering due to the edge.[8,9] These techniques also show reduced sensitivity near steep topographical transitions, such as sharp wafer edges, where electron or optical artifacts obscure meaningful signals.[10]

Coherent Fourier scatterometry (CFS) offers a promising alternative by analyzing far-field scattering patterns and extracting asymmetries with a split detector.[11] CFS has been shown to detect isolated particles as small as 100 nm on structured surfaces at the wavelength of 405 nm and provide reliable, non-contact inspection with high sensitivity to localized deviations.[12] Moreover, the use of CFS in combination with electromagnetic simulations, such as 3D finite-difference time-domain (FDTD), allows for predictive modeling of defect signal behavior

*Contact author: A.Paul-1@tudelft.nl

Optical Measurement Systems for Industrial Inspection XIV, edited by Peter Lehmann, Wolfgang Osten, Armando Albertazzi Gonçalves, Proc. of SPIE Vol. 13567, 135672I
2025 Published by SPIE · 0277-786X · doi: 10.1117/12.3062549

under different configurations.[13,14] The resulting insights enable improved interpretation of experimental results, especially in cases where edge proximity leads to complex signal overlap.[12]

In this work, we explore the resolution limitations of CFS for detecting defects close to edges. We begin with an experimental demonstration where a 200 nm Pt particle is deposited at a distance of 2 μm from a structural edge and successfully detected using CFS, while conventional SEM imaging suffers from edge artifacts. Subsequently, we employ 3D FDTD simulations to systematically vary the defect-edge distance and assess CFS signal responses for both particle and burrow defects. Our findings define the practical limits of defect detection near structural edges using CFS, bridging both experimental and numerical modeling. By quantifying how proximity to edges impacts the defect signal and understanding this behavior for different defect types, we extend CFS to edge-critical metrology. These insights contribute to the refinement of inspection methodologies where conventional techniques often fall short, particularly in the context of high-resolution, non-invasive characterization in advanced manufacturing environments.

2. METHODS

2.1 Experimental Setup

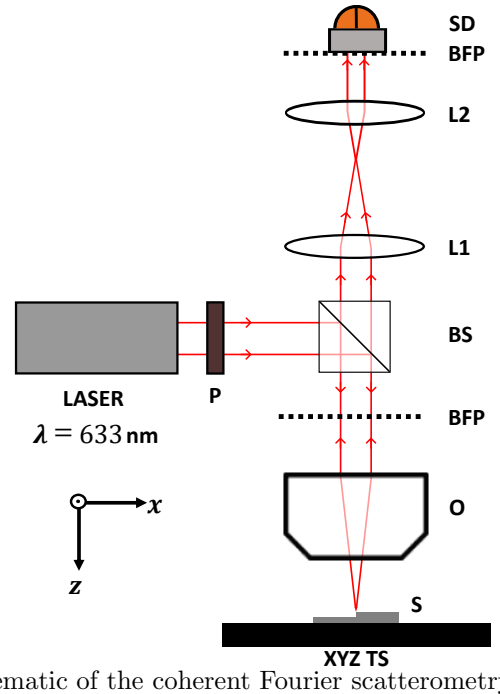

Figure 1: Schematic of the coherent Fourier scatterometry (CFS) setup.

The CFS setup (schematic as shown in Fig. 1) consists of a linearly polarized He-Ne laser source ($\lambda = 633$ nm) delivering a collimated light beam. The collimated beam is passed through a rotatable polarizer (P), then directed to a high NA (0.9) microscope objective (O) using a non-polarizing beam splitter (BS). The P can be used to control the input polarization configuration. In our experiments, we use an arbitrary polarization direction. The beam is tightly focused onto the sample surface (S), and the nominal spot size is ~ 858 nm. The sample is mounted on an XYZ piezoelectric translation stage (XYZ TS), allowing nanometer-precision lateral raster scanning. The backscattered light is collected by the same objective and redirected through the beam splitter to a 4-f optical system (L1/L2) that relays the Fourier plane (BFP) onto a custom-built split detector (SD). The differential signal, corresponding to far-field scattering asymmetries, is captured for each scan point. This configuration enables rapid, non-contact acquisition of localized scattering signatures with high sensitivity to subwavelength features.

2.2 Sample Fabrication

The sample, consisting of a Si substrate with a sharp edge, served as the substrate for particle deposition and subsequent measurements. Particle deposition is performed via electron beam induced deposition (EBID) with FEI FIB/SEM Helios G4 CX. Nominal sizes are 200×200×200 nm platinum (Pt) particles deposited 2 μm and 4 μm from the edge. The settings used: 5 kV acceleration voltage, 1.3 pA beam current, 200 ns dwell time, −90% overlap, 0.05 μm3/nC volume per dose. For the Pt material, the transverse size of the resulting particles according to the SEM image is ≈ 260 nm. The SEM measurements of the tilted plane with the particles deposited were not conclusive, and it is not possible to report the height of the final structures. We observe that for the deposition of similar particles directly on silicon wafers, the height of the resulting structures is less than the nominal structure. Also, the nominal size particles we deposited are lacking definition, effectively being not a cube but rather bumps of material.

2.3 Numerical Model

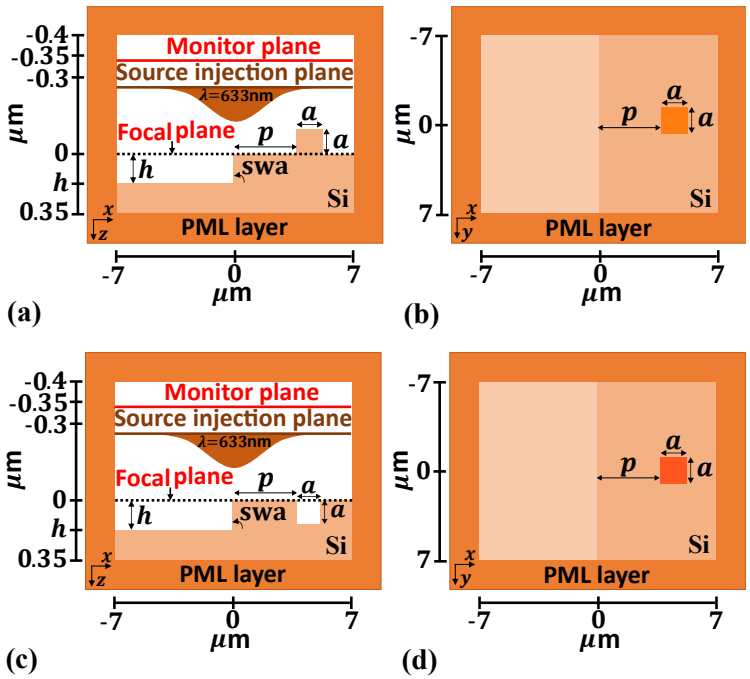

Figure 2: The 3D-FDTD simulation scheme of a defect near the edge. The edge is characterized by geometrical parameters: *swa* and h, being illuminated by a TM polarized focused spot of wavelength 633 nm and NA=0.9. The particle and the burrow are characterized by the parameters: a and p. The corresponding y = 0 plane in (a) and (c). The corresponding z = 0 plane in (b) and (d).

To model defect interactions near edges, we performed 3D FDTD simulations using Lumerical software. In fig. 2(a) and (c), the y = 0 plane, and in figure 2(b) and (d), the z = 0 plane of the complete 3D-FDTD model is depicted. The simulation domain consisted of a silicon substrate with a well-defined edge, and a cubical particle or burrow (dimension, a = 100 nm) placed at varying distances (p = 0 nm to 1000 nm) from the edge. The edge is defined by the geometrical parameters, sidewall angle, *swa* = 90°, and height, h = 100 nm. The domain was illuminated with a TM-polarized beam (λ =633 nm) focused through a 0.9 NA objective, resulting in a ∼858 nm spot size. Perfectly matched layer (PML) boundaries were used to absorb outgoing waves. Field monitors were positioned to capture near-field data, which was transformed into far-field signals. The differential signal was calculated by analyzing asymmetries across the detection plane. To simulate scanning effects, we shift the simulation object along the x-axis, keeping the position of the source injection plane, monitor plane, and computational domain constant. Simulation geometry and materials were defined in alignment with previous studies,[12,14] ensuring consistency with experimental conditions.

3. RESULTS

3.1 Experimental Detection of a Particle Near the Edge

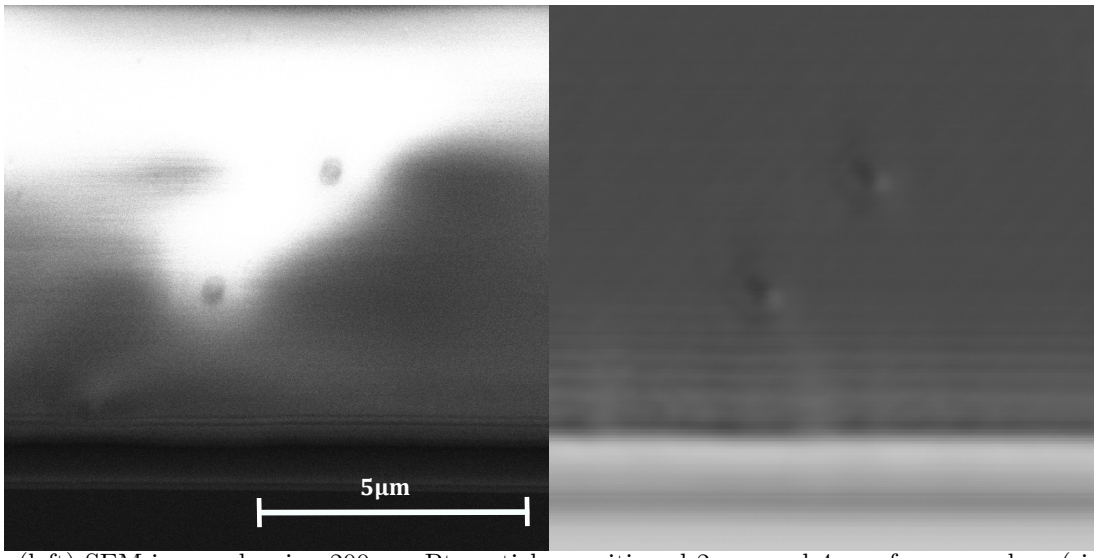

Figure 3: (left) SEM image showing 200 nm Pt particles positioned 2 μm and 4 μm from an edge. (right) CFS split detector signal mapped over the same region, detecting the fabricated Pt particles.

To investigate the feasibility of detecting particles near edges using CFS, we fabricated a sample featuring an array of 200 nm Pt particles deposited approximately 2 μm and 4 μm from a defined structural edge. Figure 3 (left) shows the corresponding SEM image, where the particles are visibly located near the edge. The proximity to the edge introduces imaging artifacts in the SEM image due to secondary electron interference, making it difficult to resolve fine features.[6] Despite this imaging challenge, CFS measurements on the same sample region reveal a clear differential signal indicating the presence of the particles. The CFS data, shown in Fig. 3 (right), presents the split detector signal intensity mapped across the scanned region. This demonstrates that CFS is capable of resolving features even in close proximity to strong scatterers such as edges, where traditional dark-field microscopy fails due to overwhelming background intensity.

This experimental result confirms that particles as close as 2 μ m to the edge can be reliably detected using CFS. However, reducing this distance further through controlled fabrication is highly challenging, which motivates the following numerical investigation into the detection limits at sub-micrometer distances.

3.2 Numerical Study: Particles Near the Edge

To systematically assess the limits of particle detection near edges, we simulated a 100 nm particle in the shape of a cube placed at varying distances ($p = 50$ nm to 1050 nm) from a sharp edge on a planar Si substrate. Using the 3D FDTD model described earlier, we computed the split detector signals corresponding to each particle-edge configuration. The illumination conditions replicated the experimental setup: a TM-polarized (perpendicular to the edge) 633 nm beam focused by a 0.9 NA objective lens. The focused spot size was approximately 858 nm, setting a theoretical resolution limit of $\sim$351 nm ($\lambda/2$NA). The far-field profiles were analyzed to extract the normalized differential signal. Figure 4 shows the resulting normalized scan profiles for each particle distance to the edge p. As the particle is moved farther from the edge, its signature in the CFS signal becomes increasingly distinguishable. For $p > 858$ nm (the spot diameter), the particle and edge produce independent scattering features, confirming the spatial resolution of CFS in this regime. As the particle moves closer to the edge, the individual particle signal begins to merge with the edge response, leading to reduced contrast and signal ambiguity.

Nevertheless, a discernible deviation from the baseline edge signal is still observable down to $p = 350$ nm; this distance is close to the diffraction limit in this configuration. It is worth noting that for particles localized at a

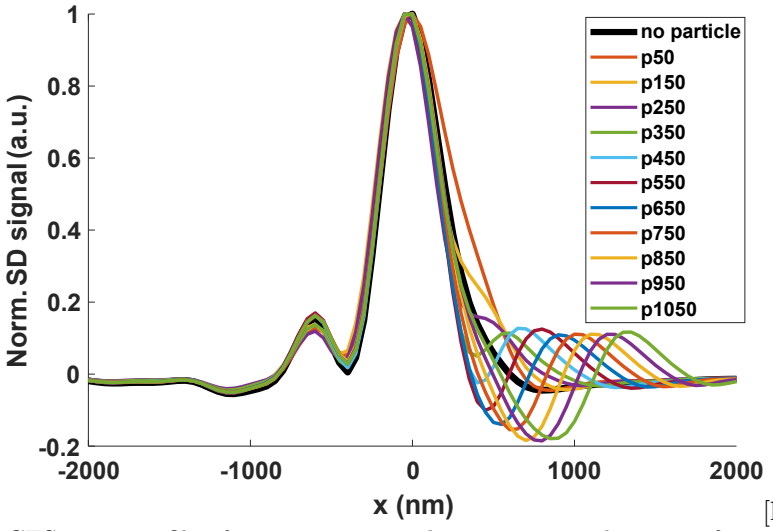

Figure 4: Simulated CFS scan profiles for 100 nm particles at varying distances from the edge (p = 50 nm to 1050 nm). As the particle distance increases, a distinct particle signal with a central zero-crossing emerges. For distances below 350 nm ($\approx$ diffraction limit of the system), the particle signal blends with the edge response, defining the system's resolution limit for particle detection. [ht!]

distance $p < 350$ nm, the CFS signal is still different from the non-particle case (black line in Fig. 4). Additional signal processing or multi-line scanning with a quad detection scheme could further enhance defect detectability within this subspot size regime.

3.3 Numerical Study: Burrows Near the Edge

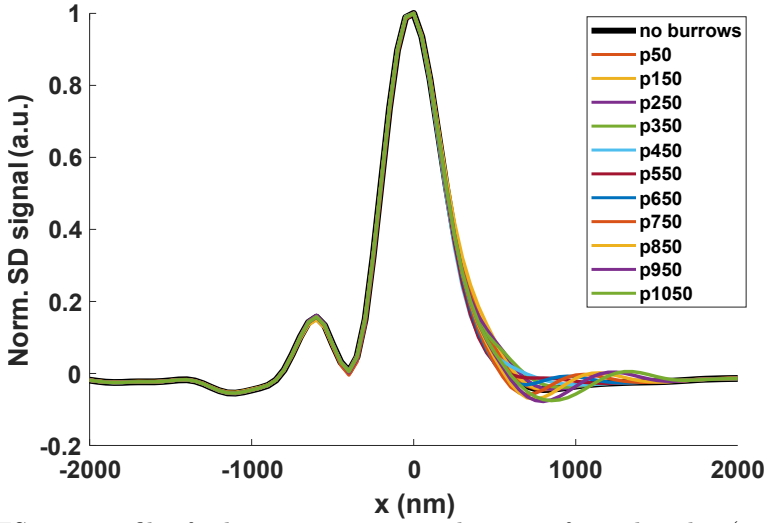

Figure 5: Simulated CFS scan profiles for burrows at varying distances from the edge (p = 50 nm and 1050 nm). Burrow signals are weaker than those of the above surface particles and exhibit a larger distance p = 650 nm, beyond which the burrow can be distinctly resolved from the edge.

To extend the defect detection analysis, we examined the detectability of subsurface burrows (voids or pits) near edges using the same 3D FDTD framework. The modeled burrows were cubical indentations with a dimension of 100 nm, placed at various lateral distances (p = 50 nm to 1050 nm) from the edge. Simulations were performed using the same TM-polarized 633 nm illumination and a 0.9 NA objective, maintaining consistency with particle simulation conditions. The far-field response was extracted from the near-field monitors and

analyzed via the split detector signal. Figure 5 shows the normalized differential signal profiles for the burrow simulations. Similar to the particle case, as the burrow is placed farther from the edge, a distinct signal emerges. However, the amplitude of the signal associated with burrows is significantly lower than that for surface particles, owing to the reduced scattering efficiency of sub-surface features. In particular, distinct burrow signals are observed until $p \geq 650$ nm, beyond which the edge and burrow signatures can be resolved separately. For $p < 650$ nm, the edge signal dominates, and the burrow's presence results only as subtle distortions in the overall profile. This suggests a larger resolution threshold for burrows compared to particles, consistent with their lower scattering cross-section.

These results highlight that while subsurface burrow detection near edges is feasible with CFS, differences in the scattered signal are smaller than for surface particles. Nonetheless, as with particle detection, multi-line scanning strategies and profile shape analysis with a quad detection scheme could help infer the presence of such defects even below the conventional resolution limit.

4. DISCUSSIONS AND CONCLUSIONS

The detection of defects near structural edges is of high relevance in semiconductor metrology and inspection, particularly as feature dimensions continue to shrink. Through a combination of experimental and numerical studies, we have evaluated the capability and limits of coherent Fourier scatterometry (CFS) in identifying both surface particles and subsurface burrows near edges. Our experimental demonstration confirms that 200 nm particles as close as 2 μm to an edge can be detected using CFS. This is a significant finding given the known challenges of strong edge-related signal interference, which tends to mask defect signatures in traditional inspection techniques such as SEM and dark-field microscopy. Numerical simulations further revealed that the minimum distance of the particle w.r.t the edge lies around 350 nm, aligning with the theoretical diffraction limit of the system with an illumination wavelength of 633 nm and Na of 0.9 ($\lambda/2NA = 351$ nm). For subsurface burrows, the minimum distance is larger (650 nm) owing to the lower scattering contrast. In both cases, as the defect-edge distance decreases below these thresholds, the individual signal becomes entangled with the edge response. However, we also observe that subtle variations in the far-field profile persist, indicating that such defects can still influence the overall measurement even when not distinctly resolved. In particular, scanning across multiple lines parallel to the edge and analyzing the profile asymmetries may allow for the detection of small particles closer to the edge. In conclusion, this study establishes resolution benchmarks for edge-adjacent defect detection using CFS and demonstrates its superiority over conventional methods in such scenarios. The findings lay the groundwork for optimizing CFS-based inspection protocols in edge-critical applications, thereby extending its utility in high-precision nanometrology.

ACKNOWLEDGMENTS

We acknowledge the Nederlandse Organisatie voor Wetenschappelijk Onderzoek (Project 17-24 Synoptics No. 2) for funding this research. The authors thank Dmytro Kolenov and Thomas Scholte of TU Delft for sample fabrication.

REFERENCES

[1] Morillo, J. D., Houghton, T., Bauer, J. M., Smith, R., and Shay, R., "Edge and bevel automated defect inspection for 300mm production wafers in manufacturing," in [*IEEE/SEMI Conference and Workshop on Advanced Semiconductor Manufacturing 2005.*], 49–52, IEEE (2005).

[2] Strapacova, T., Priewald, R., Jerman, T., and Mentin, C., "Inline wafer edge inspection system for yield enhancement of thin wafers," in [*2017 28th annual SEMI Advanced Semiconductor Manufacturing Conference (ASMC)*], 138–143, IEEE (2017).

[3] Tran, T., Roberts, W., Tiffany, J., Jekauc, I., Clements, N., Jowett, P., Ferguson, R., Mattson, D., Demmert, C., Richmond, M., et al., ""Extreme edge engineering"-2 mm edge exclusion challenges and cost-effective solutions for yield enhancement in high volume manufacturing for 200 and 300 mm wafer fabs," in [*2004 IEEE/SEMI Advanced Semiconductor Manufacturing Conference and Workshop (IEEE Cat. No. 04CH37530)*], 453–460, IEEE (2004).

[4] Frase, C. G., Buhr, E., and Dirscherl, K., "CD characterization of nanostructures in SEM metrology," *Measurement Science and Technology* **18**(2), 510 (2007).

[5] Hussain, D., Ahmad, K., Song, J., and Xie, H., "Advances in the atomic force microscopy for critical dimension metrology," *Measurement Science and Technology* **28**(1), 012001 (2016).

[6] Wells, O., "Penetration effect at sharp edges in the scanning electron microscope," *Scanning* **1**(1), 58–60 (1978).

[7] Zhu, J., Liu, J., Xu, T., Yuan, S., Zhang, Z., Jiang, H., Gu, H., Zhou, R., and Liu, S., "Optical wafer defect inspection at the 10 nm technology node and beyond," *International Journal of Extreme Manufacturing* **4**(3), 032001 (2022).

[8] Peters, L., "Defect Challenges Grow At The Wafer Edge," (2024). Available at https://semiengineering.com/defect-challenges-grow-at-the-wafer-edge/.

[9] Ali, B., "A Bare Wafer Mystery: Inspecting For Back, Edge, And Notch Defects In Advanced Nodes," (2023). Available at https://semiengineering.com/a-bare-wafer-mystery-inspecting-for-back-edge-and-notch-defects-in-advanced-nodes/.

[10] Yoshioka, T., Miyoshi, T., and Takaya, Y., "Particle detection for patterned wafers of 100nm design rule by evanescent light illumination: analysis of evanescent light scattering using finite-difference time-domain (FDTD) method," in [*SPIE Proceedings*], **6049**, 604909–, SPIE (December 2005).

[11] Kolenov, D., Zadeh, I. E., Horsten, R. C., and Pereira, S. F., "Direct detection of polystyrene equivalent nanoparticles with a diameter of 21 nm ($\lambda/19$) using coherent fourier scatterometry," *Optics Express* **29**(11), 16487–16505 (2021).

[12] Paul, A., Kolenov, D., Scholte, T., and Pereira, S. F., "Coherent Fourier scatterometry: a holistic tool for inspection of isolated particles or defects on gratings," *Applied Optics* **62**(29), 7589–7595 (2023).

[13] Paul, A., Rafighdoost, J., Dou, X., and Pereira, S. F., "Investigation of coherent Fourier scatterometry as a calibration tool for determination of steep side wall angle and height of a nanostructure," *Measurement Science and Technology* **35**(7), 075202 (2024).

[14] Paul, A., Wever, R., Soman, S., and Pereira, S. F., "Utilizing focused field as a probe for shape determination of subwavelength structures via coherent Fourier scatterometry," *Physical Review Applied* **23**(2), 024016 (2025).